

Hadronic Reaction Zones in Relativistic Nucleus-Nucleus Collisions

D. Anchishkin¹, V. Vovchenko², S. Yezhov²

¹*Bogolyubov Institute for Theoretical Physics, 03680 Kiev, Ukraine*

²*Taras Shevchenko Kiev National University, 03022 Kiev, Ukraine*

February 26, 2013

Abstract

On the basis of the proposed algorithm for calculation of the hadron reaction rates, the space-time structure of the relativistic nucleus-nucleus collisions is studied. The reaction zones and the reaction frequencies for various types of reactions are calculated for AGS and SPS energies within the microscopic transport model. The reaction zone boundaries are related to the kinetic and chemical freeze-outs. The specific characteristic time moments of the fireball evolution are introduced. It is found that the time of the division of a reaction zone into two separate parts does not depend on the collision energy. We argue that the evolution of nucleus-nucleus collision can be divided into two stages. The first stage is mainly attributed to nucleon processes with the most intensive reactions occur when two colliding nuclei fully overlap (this time moment depends on the initial nucleus velocity). The second stage is mainly attributed to secondary particles, which take part in decays, fusions, and elastic rescatterings with the most intensive reactions occurring at the time moment $t \approx 6 - 10$ fm/c for AGS and SPS energies, and the total duration of this stage gradually increases with the collision energy.

1 Introduction

In the heavy-ion collisions, a strongly interacting hadronic system is formed – a fireball. This system is identified with a space-time region, in which the intensive hadronic reactions are running. With regard for a model describing the system, we can separate such stages of the fireball evolution as the formation of a fireball, its thermalization, hydrodynamic expansion, freeze-out, etc.

As parameters for the determination of the stages of evolution of a system, one can take the particle density $n(t, \mathbf{r})$ [1, 2], energy density $\epsilon(t, \mathbf{r})$ [2, 3], temperature $T(t, \mathbf{r})$ [4, 5], mean free path, rate of collisions of particles $\Gamma(t, \mathbf{r})$, etc. The same parameters are also used for the determination of the chemical and kinetic freeze-out processes [6, 7, 8]. Depending on the chosen parameter, one can get various fireball representations. In the present work, we use the hadron reaction rate $\Gamma(t, \mathbf{r})$ (number of reactions in a unit volume per unit time) in a given four-dimensional region of the space-time as a parameter of the spatial evolution of the interacting system. Such a quantitative estimate allows one to define the reaction zone [9], which study gives a possibility to establish the space-time structure of a fireball from the viewpoint of the

interaction (collision) intensity at every point of the space-time. Then, the regions of a fireball can be distinguished by the interaction intensity that can be characterized by the number of collisions in a unit volume of the space-time. We use this quantity to estimate and to quantify various regions of the reaction zone.

Another important question which can be clarified by the study of the zone of reactions is how the space-time boundary of a particular region of the reaction zone is related to the processes of kinetic and chemical freeze-outs. Since the kinetic freeze-out is the process of establishment of a final distribution of hadrons in the momentum space, the sharp kinetic freeze-out hypersurface is an imaginary hypersurface, outside of which there are no collisions between radiated hadrons (or a very small amount of collisions is admitted). In this sense, the space-time boundary of a reaction zone and the sharp kinetic freeze-out hypersurface can be put in correspondence.

2 Reaction zones

The number of reactions N_{coll} in the given space-time region Ω can be evaluated in the following way:

$$N_{\text{coll}}(\Omega) = \int_{\Omega} d^4x \Gamma(x), \quad (1)$$

where the four-density of reactions $\Gamma(x)$ can be evaluated, in turn, in the framework of a certain model approximation, e.g., like that in [10, 11]. In particular, $\Gamma(x)$ can be calculated with the use of a distribution function $f(x, p)$ within a transport model.

The reaction zone is defined as *the space-time region where a certain fraction of all reactions of a certain type take place* [9]. This space-time region is chosen so that it should be the most intense with respect to the reaction rate, i.e., it has the smallest possible volume. Reactions are classified by the type and the number of particles taking part in these reactions (see Table 1). The reaction zone can be calculated for various types of reactions with the use of the particular rate for a given reaction type.

One can get a feeling of the definition given above, while associating the reaction zone with the flame of a candle (see Fig. 2). Indeed, it is the region that is the most intense with respect to exothermic “luminous” reactions and is basically a reaction zone (as usual, we do not care about the regions which contain the products of the oxidizing reaction that are not visible to us).

In the present paper, we investigate the most central nucleus-nucleus collisions. Because of the symmetry of central collisions, the reaction density does not depend on the azimuthal angle φ in the x - y plane in the cylindrical coordinates, i.e., $\Gamma(t, x, y, z) = \Gamma(t, r, z)$. In this case it is possible to build a three-dimensional reaction zone in coordinates (t, r, z) , where $r = \sqrt{x^2 + y^2}$.

Our task is to determine a hypersurface that confines the volume containing a certain part α ($0 < \alpha < 1$) of the total number of all hadronic reactions N_{tot} . This hypersurface can be determined by the equation

$$\Gamma(t, r, z) = \Gamma_c, \quad (2)$$

where the critical value Γ_c satisfies the equation for a given value of α

$$\int dt dx dy dz \Gamma(t, x, y, z) \theta(\Gamma - \Gamma_c) = 2\pi \int dt dr dz r \Gamma(t, r, z) \theta(\Gamma - \Gamma_c) = \alpha N_{\text{tot}}. \quad (3)$$

Table 1: **Classification of reactions**

1	$1 \rightarrow 2' + m, m \geq 0$	decay
2	$2 \rightarrow 1'$	fusion
3	$2 \rightarrow 2$	elastic scattering
4	$2 \rightarrow 2' + m, m \geq 0$	inelastic reaction

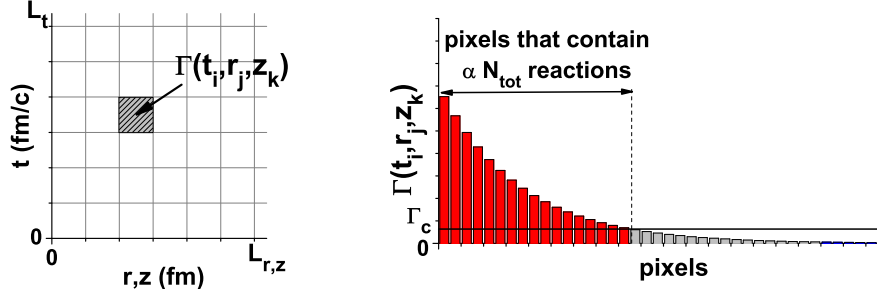


Figure 1: Algorithm for the selection of pixels in the determination of the reaction zone. Left panel: the grid of pixels in the cylindrical coordinates (t, r, z) . Right panel: the arrangement of all bins, which are put in correspondence to pixels, in a linear hierarchy in accordance with their height (the density of reactions Γ in the corresponding pixel). A value of Γ_c defines the lower (right) boundary, when we go from the very left bin (pixel with the highest density Γ) to the right along this hierarchy, see Eq. (3).

It is obvious that the value of Γ_c “determines” the “luminous” part of the reaction zone analogously to the luminous region of the flame of a candle.

To carry out evaluations, we use the microscopic transport model UrQMD v2.3 [12, 13], which allows one to calculate the four-density of reactions at every point of the space-time and to select the reactions of a necessary type and the species of particles. We take a large four-volume of reactions C_R , which is determined in the cylindrical coordinates (t, r, z) as: $0 < t < 200$ fm/c, $0 < r < 200$ fm and -200 fm $< z < 200$ fm.

To calculate the critical rate Γ_c and to determine the reaction zone, we divide the four-volume C_R into cells (pixels), i.e., elements of the four-space, as shown in Fig. 1 (left panel). Let $\Omega_{ijk} = \Omega(t_i, r_j, z_k)$ be the four-volume of a pixel with coordinates (t_i, r_j, z_k) of its center. Hence, this pixel is defined as

$$t_i - \frac{1}{2}\Delta t < t < t_i + \frac{1}{2}\Delta t, \quad r_j - \frac{1}{2}\Delta r < r < r_j + \frac{1}{2}\Delta r, \quad z_k - \frac{1}{2}\Delta z < z < z_k + \frac{1}{2}\Delta z, \quad (4)$$

where $\Delta t = \Delta r = \Delta z = 1$ fm in our calculations. The values of Δ determine the sampling accuracy in our method. The four-volume of a pixel with coordinates (t_i, r_j, z_k) is $\Omega(t_i, r_j, z_k) = 2\pi r_j \Delta t \Delta r \Delta z$. Then, for each three numbers (t_i, r_j, z_k) , which determine a certain pixel, we can calculate the reaction density $\Gamma(t_i, r_k, z_k)$ in the given pixel from UrQMD by calculating the number of reactions in that pixel and dividing it by the four-volume $\Omega(t_i, r_j, z_k)$ of the pixel. After this, we put all pixels on the line in the form of bins of equal width and of a height, which is equal to the pixel intensity $\Gamma(t_i, r_k, z_k)$. We sort the bins (pixels) from left to right by the following hierarchy: from a pair of bins (pixels), the left bin is higher (the pixel has a larger reaction density), see Fig. 1 (right panel). The total integral of $\Gamma(t, r, z)$ (the sum of Γ -values in pixels multiplied by corresponding pixel four-volume Ω) is equal to the total number of all

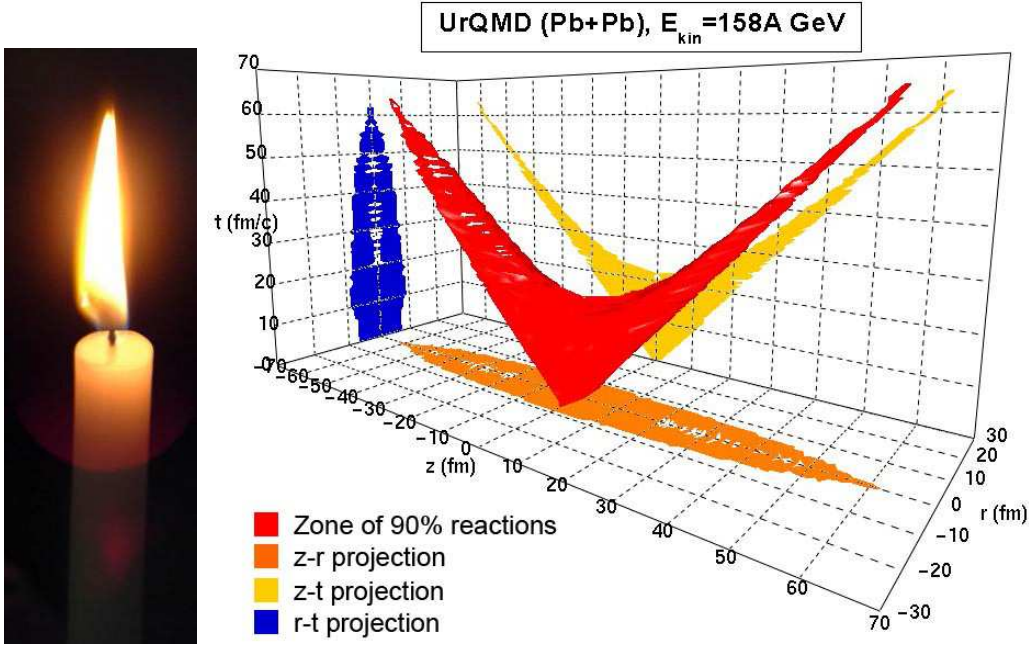


Figure 2: Left – a candle with a flame corresponding to the region, where reactions take place. Right – the three-dimensional reaction zone that determines the space-time region, where 90% of all hadronic reactions under SPS conditions ($E_{\text{kin}} = 158A$ GeV) take place.

hadron reactions N_{tot} in the four-volume of reactions C_R .

Let us sum the values of reaction densities multiplied by the corresponding Ω beginning from the left according to the obtained hierarchy. We recall that the value of each $\Gamma(t_i, r_j, z_k) \Omega(t_i, r_j, z_k)$ gives the number of reactions in the corresponding pixel. Increasing the number of pixels in the sum, we can reach the value of sum that is equal to a given number αN_{tot} , where α is a given fraction of the absolute number of all reactions N_{tot} , see Fig. 1 (right panel) and Eq. (3). For instance, for $\alpha = 0.9$ the critical density of reactions Γ_c will corresponds to the 90% of the total number of reactions. The current value of reaction density in the hierarchy at that point is $\Gamma_c(\alpha)$.

In Fig. 2, we show the calculation results under conditions at the CERN Super Proton Synchrotron (SPS), Pb+Pb at 158A GeV in the case of central collisions. The figure depicts the space-time region, where 90% of all hadronic reactions take place. For this calculations, we use the coordinates (t, r, z) , where $r = \pm\sqrt{x^2 + y^2}$. In addition, we show the different orthographic projections of the reaction zone on the coordinate planes z - t (yellow), r - t (blue), and z - r (orange).

Then we apply the same evaluation procedure to determine the three-dimensional reaction zone of the inelastic hadronic reactions ($2 \rightarrow 2' + m, m \geq 0$). In Figs. 3-5, the results of calculations under conditions at the BNL Alternating Gradient Synchrotron (AGS), Au+Au, and at the SPS, Pb+Pb, are depicted. It is seen that, at SPS energies, the reaction zone (fireball) breaks-up into two spatial parts. Meanwhile, at AGS energies, there is virtually no break-up of a fireball, but the fireball disappears almost immediately as a whole. The reaction zones in the z - r coordinates at times before and after the break-up of a fireball are also shown in Figs. 3-5.

While comparing the results of calculation for the energy $E_{\text{kin}} = 158A$ GeV for all reactions (Fig. 2) and for inelastic reactions (Fig. 5), it is obviously seen that the reaction zone containing

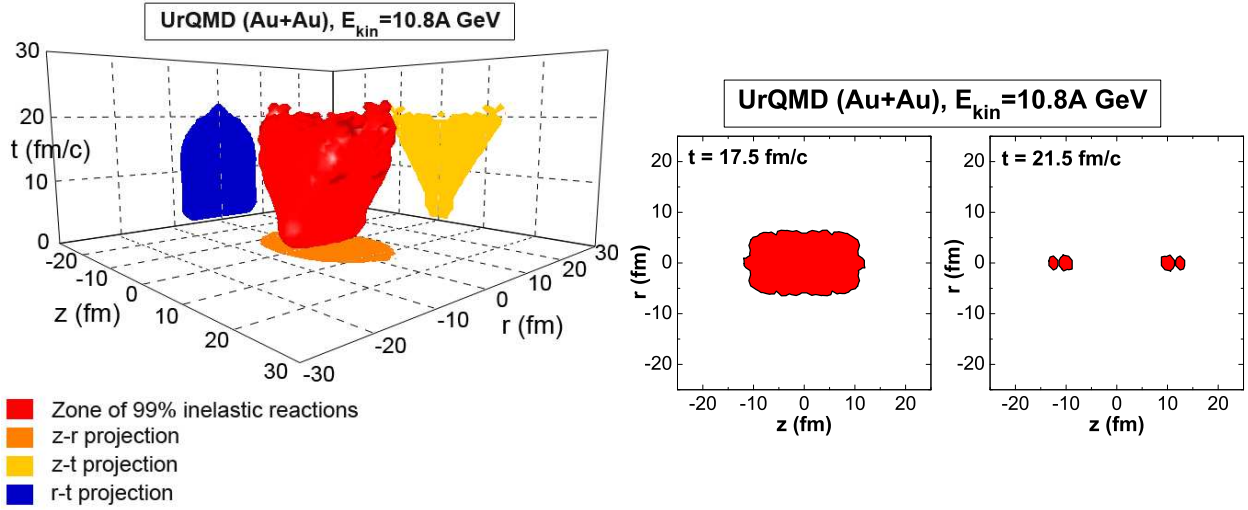


Figure 3: Left – the three-dimensional reaction zone, which determines the space-time region where 99% of all inelastic hadronic reactions under AGS conditions ($E_{\text{kin}} = 10.8A$ GeV) take place. Right – the same reaction zone in the z - r coordinates at different times before and after the hot-fireball break-up.

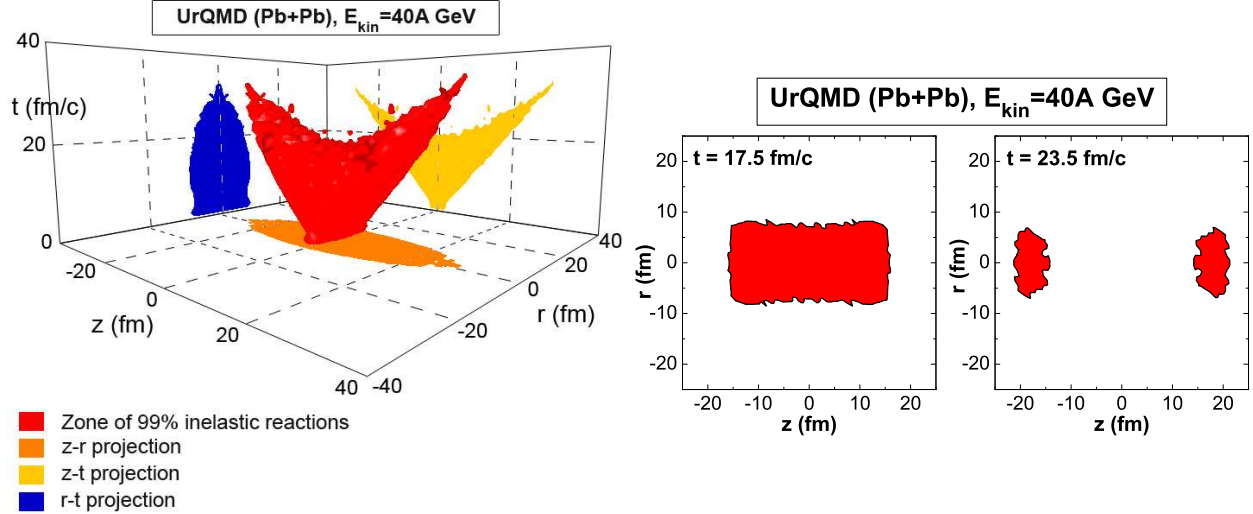


Figure 4: Same as in Fig. 3, but under SPS conditions at $E_{\text{kin}} = 40A$ GeV.

90% of all reactions roughly coincides with the reaction zone containing 99% of all inelastic reactions. We name this part of the reaction zone as a *hot fireball*. Hence, everything that is beyond a hot fireball contains approximately 10% of the total number of reactions and just 1% of all inelastic reactions.

In this study, we parameterize reaction zones by the global parameter α (fraction of the total number of reactions contained in the corresponding reaction zone), rather than the local critical inelastic reaction density Γ_c for various collision energies. We remind, that the hypersurface which separates different 4D zones is usually determined, for instance, for the density of particles as $n(t, \mathbf{r}) = n_c$; in our case this hypersurface can be determined as $\Gamma(t, \mathbf{r}) = \Gamma_c$. The parameters α and Γ_c are related to one another via Eq. (3) for each particular collision energy. It is interesting to explore this relation in greater details. The values of Γ_c for given different values of α and different collision energies are presented in Table 2. It is seen that the values of $\Gamma_c(\alpha)$

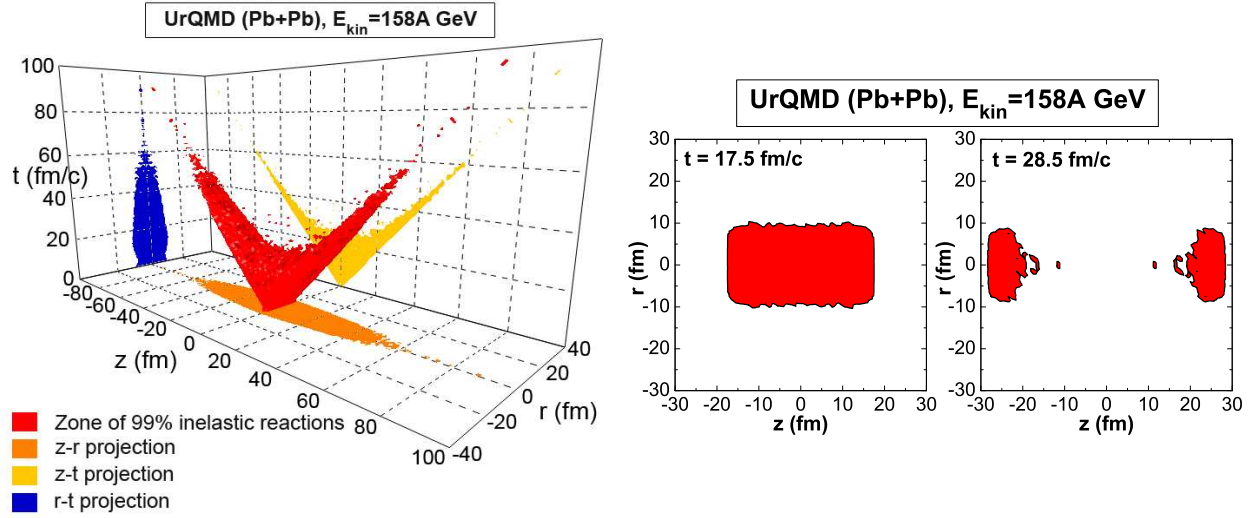


Figure 5: Same as in Fig. 3 but for SPS conditions at $E_{\text{kin}} = 158A$ GeV.

Table 2: **Critical density Γ_c of the inelastic reactions for given values of α**

E_{kin} (A GeV)	$\sqrt{s_{AA}}$ (A GeV)	$A + A$	$\Gamma_c (\alpha = 0.8)$ [fm ⁻³ · (fm/c) ⁻¹]	$\Gamma_c (\alpha = 0.99)$ [fm ⁻³ · (fm/c) ⁻¹]
10.8	4.88	$Au + Au$	$119.07 \cdot 10^{-3}$	$0.51 \cdot 10^{-3}$
20.0	6.41	$Pb + Pb$	$83.63 \cdot 10^{-3}$	$0.35 \cdot 10^{-3}$
40.0	8.86		$60.59 \cdot 10^{-3}$	$0.22 \cdot 10^{-3}$
80.0	12.39		$42.86 \cdot 10^{-3}$	$0.15 \cdot 10^{-3}$
158.0	17.32		$31.42 \cdot 10^{-3}$	$0.11 \cdot 10^{-3}$

are different at different collision energies.

Hence, our approach with fixed α (which is a global parameter) for different collision energies is not exactly equivalent to that with fixed Γ_c (which is a local quantity). However, it is seen from Table 2 that the values of Γ_c for the same given α are of the same order of magnitude for different energies, whereas the change of α from 0.8 to 0.99 leads to a change in Γ_c of two orders of magnitude. Therefore, the differences in Γ_c for different energies are not very significant. This means that the approach, where Γ_c is fixed, should yield qualitatively the same results as those in the case where the fixed quantity is α because the inverse dependence of α on Γ_c , i.e. $\alpha(\Gamma_c)$, is weak. We have performed calculations of the three-dimensional inelastic reaction zone for different energies with $\Gamma_c(\alpha = 0.99)$ values from Table 2, see Figs. 3-5. The resulting reaction zones for energies from Table 2 are roughly the same in the range of these Γ_c values, at least till the time moment when the reaction zone separates into two different spatial pieces (drops).

Henceforth, we will deal with the projection of the reaction zone on the z - t plane. To design this projection, we sum firstly all collisions along the transverse direction at the fixed coordinates (t, z) . Then, the reaction density in the z - t plane takes the form

$$\tilde{\Gamma}(t, z) = \int dx dy \Gamma(t, x, y, z) = 2\pi \int dr r \Gamma(t, r, z). \quad (5)$$

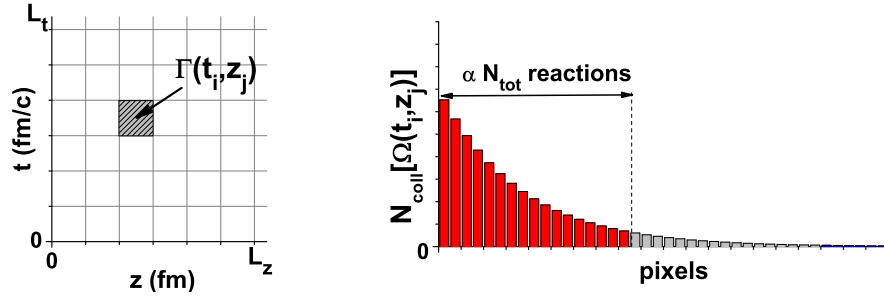


Figure 6: Algorithm for the selection of pixels in the determination of the reaction zone projection in $t - z$ coordinates. Left panel: the grid of pixels in coordinates (t, z) . Right panel: the arrangement of all bins in a linear hierarchy in accordance with their height (the height of the bin is equal to the number of reactions in the corresponding pixel).

Then the number of reactions in the given pixel $\tilde{\Omega}(t, z)$ on $z-t$ plane is

$$\tilde{N}_{\text{coll}}[\tilde{\Omega}(t, z)] = \int_{\tilde{\Omega}(t, z)} dt dz \tilde{\Gamma}(t, z). \quad (6)$$

To construct the reaction zone projection from UrQMD we divide the two-dimensional $z - t$ plane into rectangular cells (pixels) with lengths $\Delta t = 1$ fm/c and $\Delta z = 1$ fm (see Fig. 6, left panel). The volume of a pixel is then $\tilde{\Omega}(t_i, z_j) = \Delta t \Delta z$ and does not depend on values of t_i and z_j , i.e. it is the same for all pixels. It is different from the case of (t, r, z) coordinates where the four-volume of a pixel depended on transverse coordinate r . This allows us to construct the reaction zone projection with the use of the above-mentioned algorithm where in place of the pixel intensity $\Gamma(t, r, z)$, which in the previous sorting problem determined the height of the bin, we put the number of collisions in the correspondent pixel $\tilde{N}_{\text{coll}}[\tilde{\Omega}(t, z)]$, which is now the height of the bin as depicted in Fig. 6, right panel (see details in Ref. [9]).

It is worth to note that this reaction zone projection onto the $z-t$ plane does not necessarily coincide with the corresponding projections of the three-dimensional reaction zone in Figs. 3-5, which are just orthographic projections of the reaction 4-density $\Gamma(t, r, z)$. However, they are found to be roughly the same.

In Figs. 7, 8, and 9, we show the results of calculations under conditions at the BNL-AGS, Au+Au, and at the CERN-SPS, Pb+Pb, in the case of central collisions. In accordance with our algorithm, the volume that contains 60% of all hadronic inelastic reactions, $2 \rightarrow 2' + m, m \geq 0$, is determined (depicted as the yellow area). Next, we determine the volume that contains 80% of all hadronic inelastic reactions and includes the previous zone (depicted as the dark red area plus the previous area). Finally, we determine the volume that contains 99% of all hadronic inelastic reactions and also includes the previous zone (depicted as the red area plus the previous two areas). As was previously mentioned, this zone is named as the region of a hot fireball. We determine also a volume that contains 99% of all possible hadronic reactions and includes, of course, the previous zone. We name the region of 99% of all hadronic reactions excluding the zone of the hot fireball as a cold fireball (blue area).

After some time t_d , the inelastic reaction zones studied in this work either decay completely, or are spatially divided into two parts, which move away from each other in opposite directions, see Figs. 7-9. This division time t_d , which depends on the fraction α , can be defined as $t_d \equiv t_\alpha(z)|_{z=0}$, where the time dependence $t_\alpha(z)$ defines the border between two reactions

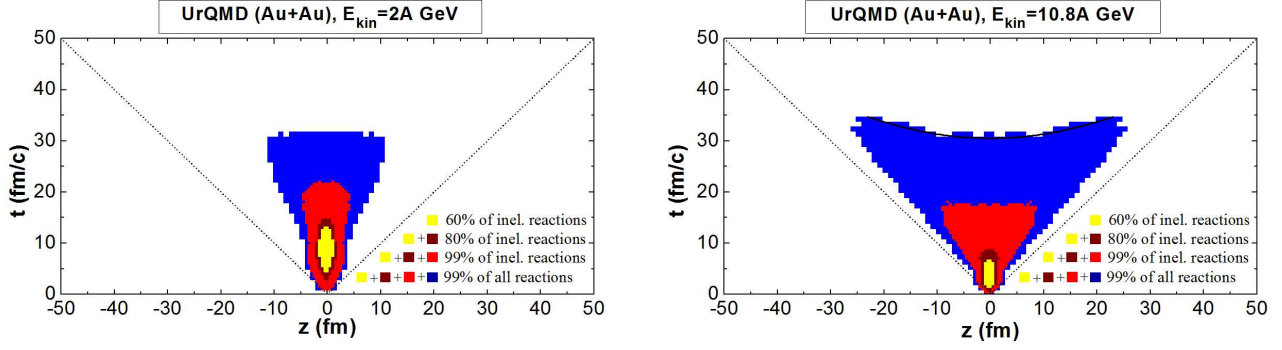


Figure 7: Projection of the reaction zone on the z - t plane under the AGS (Au+Au at 2A GeV and 10.8A GeV) conditions. The yellow region contains 60% of all inelastic reactions, $2 \rightarrow 2' + m, m \geq 0$. The dark red region together with previous region contains 80% of all inelastic reactions. The red region together with the previous region contains 99% of all inelastic reactions. The blue region together with the previous region contains 99% of all hadronic reactions.

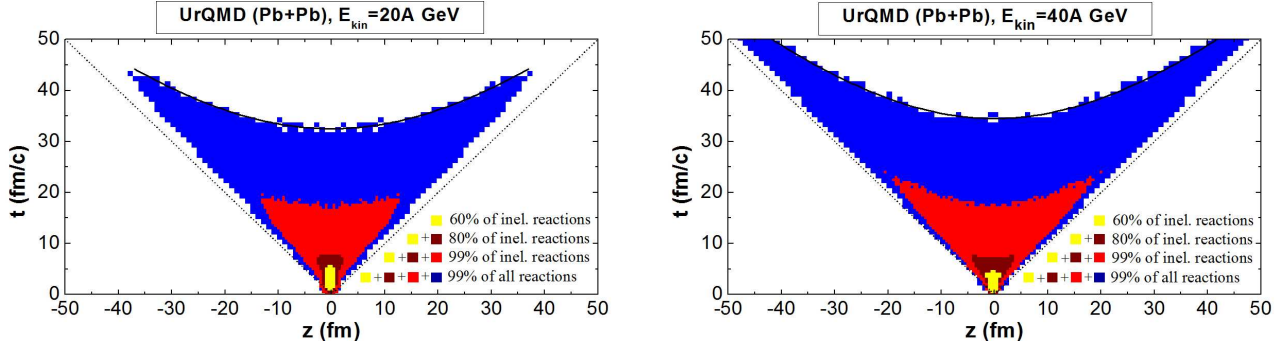


Figure 8: Same as in Fig. 7, but for calculations under low SPS conditions (Pb+Pb at 20A GeV and 40A GeV).

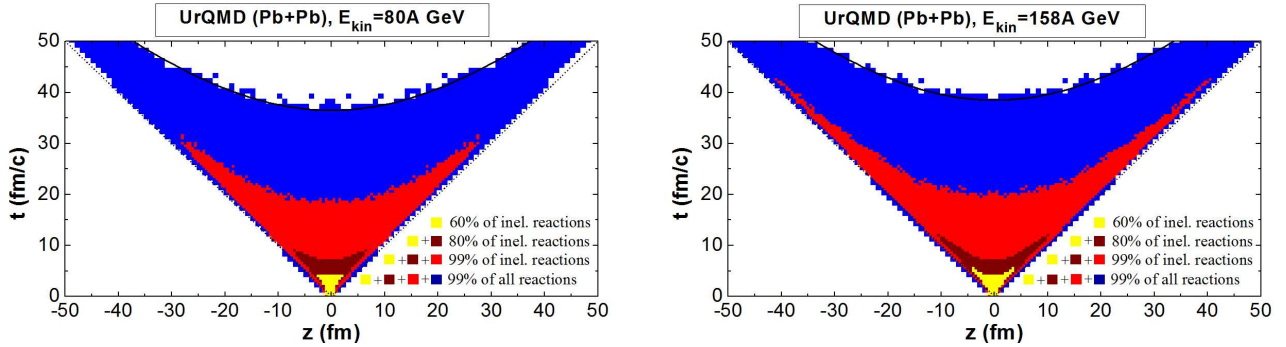


Figure 9: Left and center – same as in Fig. 7, but for calculations under SPS conditions (Pb+Pb at 80A GeV and 158A GeV).

zones. For details see Fig. 10 which represent in big scale the corresponding reaction zone in the central region. The values of t_d for different values of α and different collision energies are depicted in Table 3.

One of the main features seen from Table 3 is that the division time t_d of a separation of the particular reaction zone into two different spatial parts depends weakly on the collision energy for different values of α . That is especially true for higher values of α and in the case where

Table 3: Division time t_d of the inelastic reaction zone for given values of α

E_{kin} (A GeV)	$\sqrt{s_{AA}}$ (A GeV)	$t_d(\alpha=0.6)$ (fm/c)	$t_d(\alpha=0.8)$ (fm/c)	$t_d(\alpha=0.99)$ (fm/c)
10.8	4.88	6.5	8.5	17.5
20.0	6.41	5.5	7.5	17
40.0	8.86	4.5	7	17.5
80.0	12.39	4.25	7	18
158.0	17.32	4.25	7	19.5

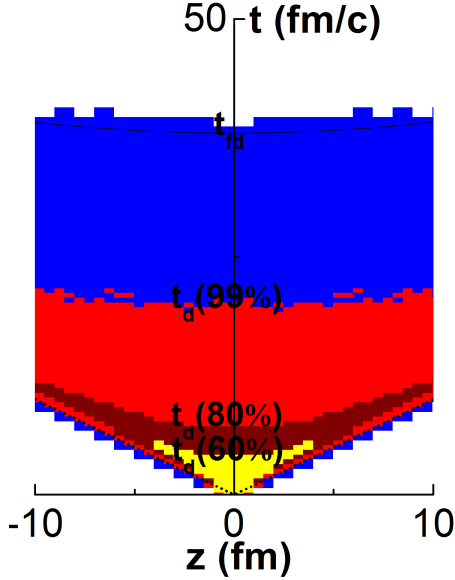


Figure 10: Central part of the reaction zones under SPS conditions (Pb+Pb at 158A GeV), where the inelastic reaction zone division times t_d are indicated for different values of $\alpha \times 100\%$: 60%, 80%, and 99%.

the reaction zones are divided into two parts at t_d , rather than in the case where they would decay completely (see Figs. 7-9).

Similar result was also reported in studies of space-time structure of multipion system created in heavy-ion collisions [2]. In that work the hypersurfaces which correspond to some invariant constant densities were studied. These hypersurfaces are defined by equations $n(t, \mathbf{r}) = n_c$ and $\epsilon(t, \mathbf{r}) = \epsilon_c$, where n_c is the critical number density and ϵ_c the critical energy density of pi-mesons created in heavy-ion collision. It was found that for each particular value of critical density n_c (or ϵ_c), the division time t_{fd} depends weakly on collision energy similarly to the case of reaction zones studied in this work. These results indicate that *the weak dependence of fireball division time t_{fd} on collision energy is a universal feature of space-time structure of heavy-ion collisions.*

The zone including the hot and cold fireballs together contains 99% of all reactions by definition (see the colored area in Figs. 7-9). We can compare this reaction zone with the zone which is wrapped by the freeze-out hypersurface. Following the “classical” definition of the sharp kinetic freeze-out hypersurface, it is some boundary that separates the interacting system from the space-time domain, where the particles do not interact, and almost all particles are evaporated (frozen out) from the thin space-time layer determined by this hypersurface. Then, it seems evident that the sharp kinetic freeze-out hypersurface should be inside the reaction zone, rather than outside it. In addition, we note that the sharp chemical freeze-out hypersurface should be inside the hypersurface that separates the region of a hot fireball containing 99% of all inelastic reactions which corresponds to the area covered by the first three

Table 4: **Parameters of τ -const. hyperbola(space-like boundary of cold fireball)**

E_{kin}	t_{RZ}^0 (fm/c)	τ_{RZ} (fm/c)
10.8 (AGS)	-30	60.5
20 (SPS)	-20	52.5
40 (SPS)	-14	48.5
80 (SPS)	-8	44.5
158 (SPS)	-5	43.5

zones together depicted in Figs. 7-9.

In the coordinates (t, z) , the curve which is the upper space-like boundary of the cold fireball (“blue” zone) can be well approximated as a $\tau_{\text{RZ}} = \text{const}$ hyperbola originating from a possibly different time, t_{RZ}^0 , than the initial time $t = 0$ of the collision. This approximation was already used to describe the $[t, z]$ -projection of hypersurface of constant invariant pion density [2]. The equation for this hyperbola has the form

$$t_{\text{RZ}}(z) = t_{\text{RZ}}^0 + \sqrt{\tau_{\text{RZ}}^2 + z^2}. \quad (7)$$

The fireball division time t_{fd} is related to hypersurface parameters as

$$t_{\text{fd}} = t_{\text{RZ}}^0 + \tau_{\text{RZ}}. \quad (8)$$

The values of parameters τ_{RZ} and t_{RZ}^0 for different energies are presented in Table 4. It is seen that the parameter t_{RZ}^0 takes negative values and approaches zero with increase of the collision energy. In that case, the reaction zone boundary can be regarded as the hypersurface of a constant proper time τ_{RZ} , which originates from initial time $t = 0$ and which is then equal to t_{fd} .

The upper space-like boundary of the “blue” zone can be parameterized in a different way. For instance, it can be approximated as a hyperbola of the form $t(z) = A\sqrt{\tau_0^2 + z^2}$ [9], where $A = 0.65$, $\tau_0 = 46$ fm/c at the AGS energy ($E_{\text{kin}} = 10.8A$ GeV) and $A = 0.8 - 0.95$, $\tau_0 = 38 - 42.5$ fm/c at the SPS energies ($E_{\text{kin}} = 20 - 158A$ GeV). Here, parameter A approaches unity with increase of the collision energy, and the space-like boundary takes the form of the hypersurface of a constant proper time τ_0 , which originates from initial time $t = 0$ and coincides with previous parametrization at high energies. At AGS and SPS energies, however, the space-like boundary has a more complex structure and both parameterizations can be used to describe it.

The time-like hypersurface bounding cold fireball from below has the form of a straight line $t(z) = t_0 + \frac{1}{v}z$, where t_0 is close to zero, and $v = 0.8$ at AGS energies and $v = 0.88 - 0.98$ at SPS energies (v increases with the collision energy). At AGS energies, the time-like boundaries of the reaction zones differ significantly from one another and the light cone (see Fig. 7). However, at higher SPS energies (for example, at $E_{\text{kin}} = 158A$ GeV), the time-like hypersurfaces bounding all three zones of a fireball practically coincide with one another and are close to the light cone (see Fig. 9). Thus, we can predict that time-like hypersurfaces which bound different reaction zones from below merge at the energies available at the Relativistic Heavy Ion Collider or Large Hadron Collider and virtually coincide with the light cone.

3 Temporal structure of reactions

The structure of hadronic reactions in a fireball can be analyzed within UrQMD, which allows one to calculate the reaction density for various types of reactions.

The reactions can be classified by the type and the number of participants in a reaction (see Table 1), and the contributions of different types of reactions to the system evolution can be explored. For this purpose, we analyze the time dependence of the reaction frequency for different types, i , of reactions:

$$\nu_i(t) = \int_{C_R} dx dy dz \Gamma_i(t, \mathbf{r}). \quad (9)$$

The results of evaluations of the time dependence of the reaction frequency (9) at the AGS and SPS energies are depicted in Figs. 11, 12 and 13. The thick solid line indicates all reaction rates in a fireball, the thin solid line indicates only the elastic scattering of hadrons ($2 \rightarrow 2$), the dash-dotted line shows all inelastic reactions ($2 \rightarrow 2' + m$, where $m \geq 0$), the dotted line stands for fusion reactions ($2 \rightarrow 1'$), and the dashed line distinguishes decays ($1 \rightarrow 2' + m, m \geq 0$).

The main feature of the reaction frequency (thick solid lines in Figs. 11-13) is its increase up to $t \simeq 3.9 - 8$ fm/c at AGS energies and $t \simeq 0.84 - 2$ fm/c at SPS energies where it has its first maximum t_{m1} . This can be explained by an increase of the number of nucleons as participants of the reactions, when one nucleus penetrates into another one. Indeed, the maximum overlap of two nuclei happens, when their centers coincide. This time can be estimated as

$$t_c = \frac{R_0}{\gamma} \frac{1}{v}, \quad (10)$$

where R_0 is the nucleus radius, $v = p_{0z}/\sqrt{M_N^2 + p_{0z}^2}$, $\gamma = 1/\sqrt{1 - v^2}$, p_{0z} is the initial nucleon momentum in the c.m. system of two nuclei, and M_N is the nucleon mass. We call t_c as the fireball formation time. The values of t_c (see Table 5) are very close to the time moments that correspond to the first maximum of the reaction frequency (thick solid lines in Figs. 11-13). A slight difference of t_c and the time point of the real maximum can be explained by some decrease of the nucleon velocity, which is due to inelastic and elastic reactions (stopping) of nucleons.

As it is seen in Figs. 11-13, for all energies, the inelastic and elastic nucleon collisions dominate at the first stage, $t < t_c$, of a nucleus-nucleus collision. At later times, the elastic, decay, and fusion reactions become more significant. We note that, under all energy conditions, the decay processes become the dominant ones after $t \sim 10$ fm/c.

We also note that the maximum in the time dependence of decay reactions and, to a less extent, of fusion reactions gradually increases with the collision energy and lies in the range

Table 5: **Temporal characteristics of reaction frequency.**

E_{kin} (A GeV)	$\sqrt{s_{AA}}$ (A GeV)	$A + A$	t_c (fm/c)	t_{m1} (fm/c)	t_{m2} (fm/c)	t_{fd} (fm/c)
2.0	2.70	$Au + Au$	7.66	9.7		33.0
10.8	4.88		3.30	3.9		30.5
20.0	6.41	$Pb + Pb$	2.46	2.73	6.1	34.0
40.0	8.86		1.74	1.85	6.7	34.5
80.0	12.39		1.23	1.27	8.2	35.0
158.0	17.32		0.87	0.88	10.3	38.5

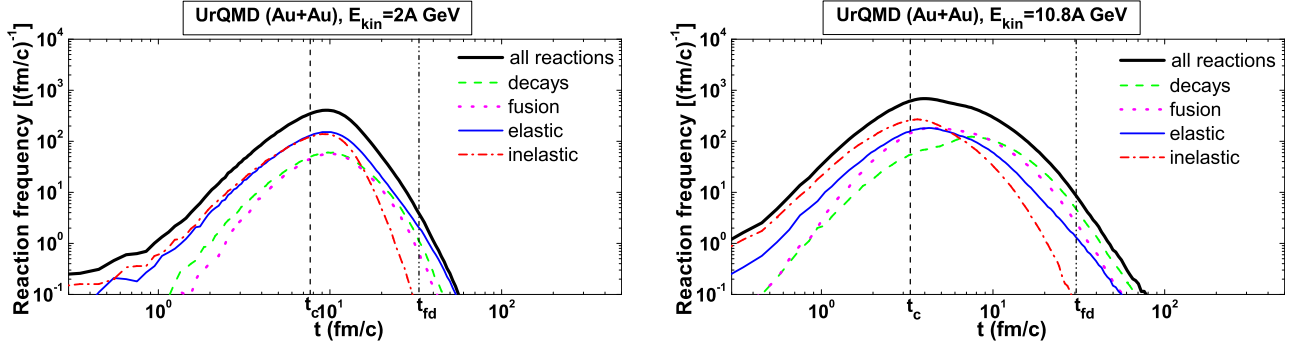


Figure 11: Hadron reaction frequency under AGS conditions (Au+Au at 2 and 10.8A GeV). Different curves correspond to different types of reactions.

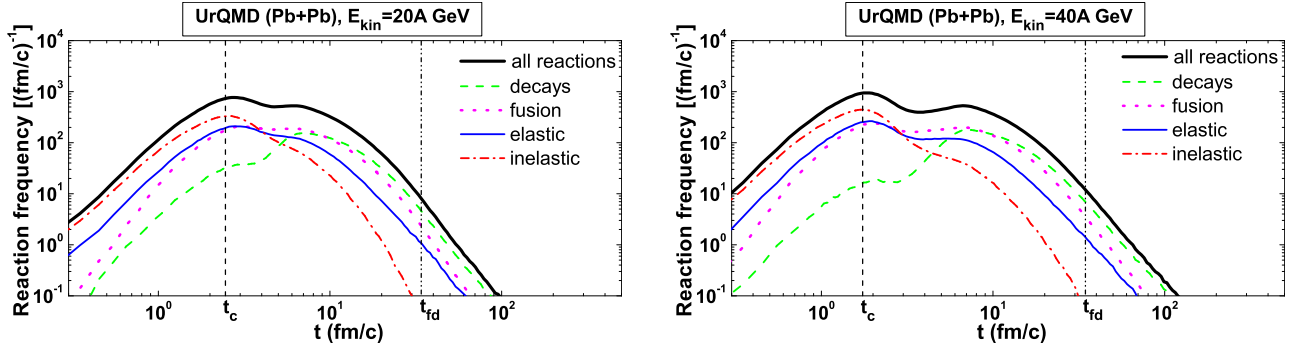


Figure 12: Same as in Fig. 11, but for calculations under low SPS conditions (Pb+Pb at 20A GeV and 40A GeV).

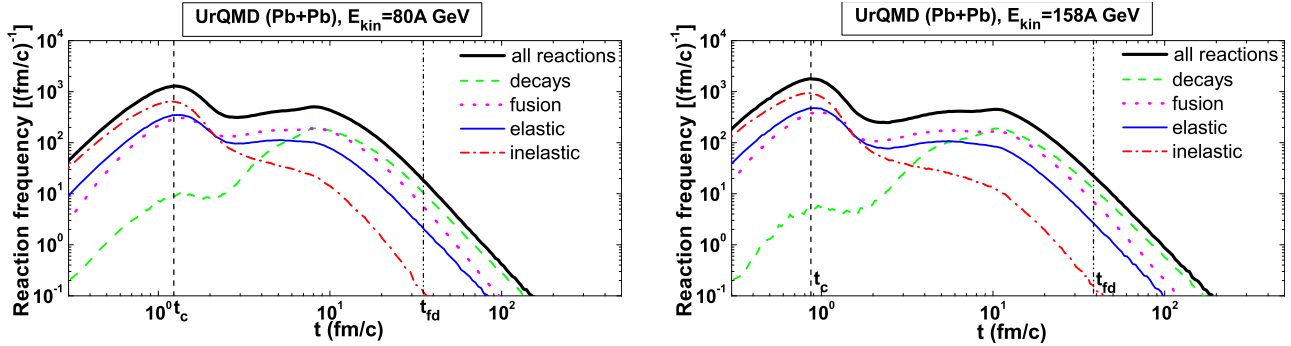


Figure 13: Same as in Fig. 11, but for calculations under SPS conditions (Pb+Pb at 80A GeV and 158A GeV).

6 – 10 fm/c at AGS and SPS energies. This rather weak energy dependence of the second maximum compared to the first maximum of reaction frequency can be attributed to the fact that the decays are mainly determined by individual properties of secondary particles rather than by the collective dynamics of a hadronic system. At AGS energies, the elastic and inelastic nucleon reactions are still most dominant in that time range, and the total reaction frequency is mostly determined by those processes. After the full overlap of the nuclei, the created system begins to expand in space, which results in a decrease of the reaction frequency under AGS conditions, as the nucleon reactions and the reactions involving secondary particles become less and less intense.

The structure of the reaction frequency changes at higher energies available at SPS. As the

collision energy increases, the maximum overlap of colliding nuclei happens at earlier times (see Eq. (10) and Figs. 12-13) due to a bigger initial velocity and the Lorentz contraction of colliding nuclei, while the processes involving secondary particles (mainly, decays and fusions) are most intense at later times in an interval of $6 - 10 \text{ fm}/c$. This indicates a clearer separation in time between the intense inelastic and elastic reactions involving net nucleons and the decay and fusion reactions, which involve secondary particles. The total contribution of the secondary particles becomes more significant at SPS energies due to an increase of the number of secondary particles with the collision energy. The number of secondary particles (mainly π mesons) is approximately $\langle n_\pi \rangle \simeq 0.6 - 1.6$ per nucleon under AGS conditions [14] and $\langle n_\pi \rangle \simeq 2 - 6$ under SPS conditions [15, 16]. For these reasons, there appears the second local maximum of the reaction frequency at SPS energies (see the thick solid line in Figs. 12 and 13) at $t = t_{m2}$ (see Table 5), which coincides with the local maxima of the decay and fusion reactions and is a consequence of a large number of reactions with secondary particles and the clearer temporal separation of processes involving the reactions between nucleons and the reactions involving secondary particles. Naturally, we come to the prediction concerning higher energies. With increase of the collision energy, the total frequency of hadron reactions will be well separated into two parts: 1) Starting from the beginning of a nucleus-nucleus collision, we can recognize the first stage that is due to nucleon-nucleon collisions. The maximum of the frequency of these collisions at $t = t_{m1}$ occurs, when the centers of the colliding nuclei coincide with each other, and this time moment can be estimated as $t_{m1} \approx t_c = R_0/(\gamma v_0)$; 2) The second stage of evolution is mainly attributed to the reactions involving secondary particles. The maximum of the total frequency of hadron reactions t_{m2} is mainly determined by the maxima of the decay and fusion reaction frequencies, and the total duration of the second stage gradually increases with collision energy.

At later times after $t = t_{m2}$, the reaction frequency goes down, which results in the division of a fireball into two spatial parts at the time moment $t = t_{fd}$ and in the further breakup. The fireball division time is defined as the minimum value of time on the space-like hypersurface, which bounds the region of the cold fireball (blue area) from above, i.e., $t_{fd} \equiv t(z)|_{z=0}$ (see Figs. 7-9). We note that the time moment t_{fd} depends weakly on the collision energy (see Table 5). It is seen that, after the time moment t_{fd} , the rates of elastic and inelastic reactions vanish. In other words, the system behavior is determined since this moment mainly by the individual properties of particles (basically, by resonances). That is why, in spite of the sufficient difference of collision energies of the experiments under consideration, the times t_{fd} are approximately the same (see Table 5). For this reason, the longitudinal size of the fireballs $2R_z$ at the time moment of division into two separate parts, $t = t_{fd}$, are approximately the same and equal to $R_z \approx v t_{fd}$ [v is defined in Eq. (10), see Figs. 7-9]. This fact can explain the weak dependence of the pion interferometric radius R_L on the beam energy [17, 18] because $R_L \propto R_z$. So, it can be claimed that the fireball achieves its maximum longitudinal size as one spatial object at the time moment $t = t_{fd}$, when it is divided into two different spatial parts.

4 Discussion and conclusions

Different parameters such as the energy density, particle density, mean free path, etc., can be used to analyze the fireball evolution. Our approach allows one to investigate the spatial and temporal structures of the hadron system created in relativistic nucleus-nucleus collisions in terms of hadronic reactions that occur in the system. In other words, the fireball is identified

as a system of interacting hadrons. The proposed algorithm gives possibility to separate, with a given accuracy, the space-time region, where the most intense hadron reactions take place, i.e. we give the method to see a reaction zone in the 3D representation (see Fig. 2) and in different projections.

In the present microscopic study, we separate a fireball into the following regions, which characterize its evolution (see Figs. 7-9): (1) a fireball region, where 60% of all inelastic hadronic reactions have occurred (yellow area), (2) a fireball region, where 80% of all inelastic hadronic reactions have occurred (yellow plus dark-red area), (3) a hot fireball region, where 99% of all inelastic hadronic reactions have occurred (yellow plus dark-red plus red area), (4) a cold fireball region (blue area), which together with the hot fireball contains 99% of all hadronic reactions N_{tot} . The last region (blue area in Figs. 7-9) contains the hadron-resonance gas, and the reactions in this region are mainly presented by decays of resonances if we consider times $t \geq t_{\text{fd}}$, see Figs. 11-13.

The study of hadron reaction zones allows one to analyze the freeze-out process in relativistic nucleus-nucleus collisions. Indeed, in the literature, the sharp freeze-out hypersurface is usually defined with the help of some parameter $P(t, \mathbf{r})$, which takes the critical value P_c on the hypersurface, i.e. the equation for that hypersurface reads as $P(t, \mathbf{r}) = P_c$. For instance, this quantity can be chosen as particle density $n(t, \mathbf{r})$ [1, 2], energy density $\epsilon(t, \mathbf{r})$ [2, 3], temperature $T(t, \mathbf{r})$ [4, 5], etc. Moreover, the “classical” definition of sharp kinetic freeze-out assumes the Cooper–Frye picture [19]: a radiation of free particles or the freeze out process takes place within a thin layer determined by a freeze-out hypersurface; this approach is usually used to describe transition from the fluid dynamical stage of heavy-ion collision to the stage of dilute hadron gas. That is why, the initial value problem for the radiation of free hadrons is formulated with the use of the space-like piece of the hypersurface, whereas the boundary conditions are formulated exploiting the time-like part of the hypersurface. Thus, the knowledge of the freeze-out hypersurface is important for estimation of the spectrum of secondary particles, for instance pions. On the other hand, if we determine the reaction zone as that containing, for example, 99% of all reactions, then we can claim that the sharp kinetic freeze-out hypersurface should be definitely inside this zone (see Figs. 7-9). Indeed, as was found in [2] the pion freeze-out hypersurface which is calculated from equation $n_\pi(t, \mathbf{r}) = n_c$, where $n_c = 0.08 \text{ fm}^{-3}$, approximately coincide with the hypersurface which bounds reaction zone that contains 80% of all inelastic hadronic reactions. (Here the value of n_c is chosen from the condition that the freeze-out size of the pion system is to be adequate to known HBT radius.)

Assuming that the chemical freeze-out occurs, when the inelastic reactions are completed (see Ref. [20]), we can also claim that the chemical freeze-out hypersurface should be inside the reaction zone, which contains 99% of all inelastic reactions.

By studying the time dependence of the reaction frequency for different reaction types, we conclude that the total reaction rate is dominated by elastic and inelastic hadron collisions at the early stage, whereas the individual properties of particles (basically, resonances) and reactions involving secondary particles determine the behavior of the system at later stages. These two stages become well separated with increase of collision energy. The first stage is characterized by the fireball formation time t_c which is defined as the time of the full overlap of two nuclei and thus it is determined by collision energy [Eq. (10)]. With increase of collision energy this time moment is a good estimation of the time moment t_{m1} , which is a maximum of nucleon-nucleon reaction frequency. The second stage is attributed mainly to decay and fusion reactions which are most intense at time moment t_{m2} (see Table 5), and the total duration of this stage increases with collision energy. Hence, the features of the second stage are mainly

determined by the individual properties of secondary particles. Another specific time point in the evolution of a hadron fireball is the fireball division time t_{fd} , which corresponds to the separation of the fireball into two different spatial parts and depends weakly on the collision energy (see the last column in Table 3).

Acknowledgements

Authors are thankful to L. Csernai for useful discussions. D.A. was supported by the program “Microscopical and phenomenological models of fundamental physical processes at micro and macro scales” (Section of physics and astronomy of the NAS of Ukraine).

References

- [1] D. Adamova *et al.* (CERES Collaboration), Phys. Rev. Lett. **90**, 022301 (2003) [arXiv:nucl-ex/0207008].
- [2] D. Anchishkin, V. Vovchenko and L.P. Csernai, Phys. Rev. C **87**, 014906 (2013) [arXiv:1211.1927 [nucl-th]].
- [3] V.N. Russkikh and Y.B. Ivanov, Phys. Rev. C **76**, 054907 (2007) [arXiv:nucl-th/0611094].
- [4] H. von Gersdorff, L. McLerran, M. Kataja, and P.V. Ruuskanen, Phys. Rev. D **34**, 794 (1986).
- [5] P. Huovinen, Eur. Phys. J. A **37**, 121 (2008) [arXiv:0710.4379 [nucl-th]].
- [6] J. Cleymans, H. Oeschler, K. Redlich, and S. Wheaton, Phys. Rev. C **73**, 034905 (2006) [arXiv:hep-ph/0511094].
- [7] B.I. Abelev *et al.* (STAR Collaboration), Phys. Rev. C **79**, 034909 (2009).
- [8] M.M. Aggarwal *et al.* (STAR Collaboration), Phys. Rev. C **83**, 034910 (2011) [arXiv:1008.3133 [nucl-ex]].
- [9] D. Anchishkin, A. Muskeyev, and S. Yezhov, Phys. Rev. C **81**, 031902 (2010) [arXiv:1004.0431 [nucl-th]].
- [10] B. Tomasik and U.A. Wiedemann, Phys. Rev. C **68**, 034905 (2003) [arXiv:nucl-th/0207074].
- [11] C.M. Hung and E. Shuryak, Phys. Rev. C **57**, 1891 (1998) [arXiv:hep-ph/9709264].
- [12] S.A. Bass *et al.*, Prog. Part. Nucl. Phys. **41**, 255 (1998) [arXiv:nucl-th/9803035].
- [13] M. Bleicher *et al.*, J. Phys. G **25**, 1859 (1999) [arXiv:hep-ph/9909407].
- [14] J.L. Klay *et al.* (E895 Collaboration), Phys. Rev. C **68**, 054905 (2003) [arXiv:nucl-ex/0306033].
- [15] C. Alt *et al.* (NA49 Collaboration), Phys. Rev. C **77**, 024903 (2008) [arXiv:0710.0118 [nucl-ex]].

- [16] S.V. Afanasiev *et al.* (NA49 Collaboration), Phys. Rev. C **66**, 054902 (2002) [arXiv:nucl-ex/0205002].
- [17] C. Adler *et al.* (STAR Collaboration), Phys. Rev. Lett. **87**, 082301 (2001) [arXiv:nucl-ex/0107008].
- [18] J. Adams *et al.* (STAR Collaboration), Phys. Rev. C **71**, 044906 (2005) [arXiv:nucl-ex/0411036].
- [19] F. Cooper and G. Frye, Phys. Rev. D **10** 186 (1974).
- [20] U. Heinz, Nucl. Phys. A **661**, 349 (1999) [arXiv:nucl-th/9907025]; Nucl. Phys. A **685**, 414 (2001).